EXPERIMENTAL COMPARISON ON MECHANICAL PROPERTIES, MICROSTRUCTURAL CHANGES AND HEAT-AFFECTED-ZONE (HAZ) SIZE OF TIG- AND LASER WELDED EN AW 6082-T6

A.M. Najib[1*], E.R. Imam Fauzi[2,3], B. Umroh[4] and M.S. Rusdi[2]

[1]Fakulti Teknologi dan Kejuruteraan Industri dan Pembuatan, Universiti Teknikal Malaysia Melaka, Hang Tuah Jaya, 76100 Durian Tunggal, Melaka, Malaysia.

[2]Manufacturing Engineering Group, School of Mechanical Engineering, Universiti Sains Malaysia, 14300 Nibong Tebal, Penang, Malaysia.

[3]Emaker Technologies, 7-13, Jalan PKAK 1 & 2, Pusat Komersial Ayer Keroh, 75450 Ayer Keroh, Melaka, Malaysia.

[4]Faculty of Engineering, Universitas Medan Area, Jalan Kolam No. 1, 20223 Medan Estate, Indonesia.

*Corresponding Author's Email: najibali@utem.edu.my

Article History: Received 2 June 2024; Revised 18 November 2024; Accepted 30 November 2024

ABSTRACT: The heat-affected zone (HAZ) reduces 30%-50% of mechanical strength in a welded 6000 series of aluminium components. The softening phenomenon of welded aluminium is not adequately addressed in current design standards such as Eurocode 9 and the British Standard Institution (BSI) Standard. In the present study, comprehensive experimental work is conducted to investigate the influence of welding methods and parameters on the occurrence of HAZ. Through experimental analysis of tungsten inert gas (TIG) and laser welding coupons, the severity and extension of HAZ were compared using tensile strength, hardness values and microstructure distribution. It is evident that tensile strength and hardness values of welded components significantly depended on heat input, welding speed, and welding method. The strength

reduction in laser-welded components was inconsistent with that of TIG-welded components. However, the extent of HAZ was much narrower in laser-welded components than in TIG welding. The grain size significantly increased after the welding process due to the fusion process. The orientation of the grain was found to be different for each welding method and was greatly influenced by the welding speed and temperature gradient of the weld pool. A comparitive analysis of mechanical and microstructural properties in TIG and laser-welded components can provide a basis to further improve the current design standards, particularly on the softening factor of welded joining. The results will significantly contribute to the enhancement of welding quality in the industrial joining practice.

KEYWORDS: *TIG, laser welding, aluminium alloy, HAZ, microstructural analysis*

1.0 INTRODUCTION

Fusion welding, including TIG and laser welding, creates three regions: the fusion zone (FZ), partially melted zone (PMZ), and heat-affected zone (HAZ). In heat-treatable alloys like EN AW 6082-T6, HAZ softening involves dissolving strengthening phases and forming incoherent precipitates. In FZ, microstructures are completely melted with temperatures above the alloy's melting point. The PMZ, on the other hand, experiences maximum temperatures ranging from the eutectic temperature to the alloy's melting temperature. Meanwhile, the HAZ, commonly referred to as the softest region adjacent to the weld, is defined as the region where the hardness values fall in the range of 30%-90% of the base metal. This region has its maximum temperature below the eutectic temperature of the alloy. For this reason, microstructures do not melt completely. Instead, they are exposed to intense heat and undergo changes during the welding process. In the case of a heat-treatable alloy such as EN AW 6082-T6, softening in HAZ involves the dissolution of the strengthening phases and the formation of incoherent precipitates [1-3]. The response to the welding process is complicated because peak temperature and time experienced during welding significantly influence the hardening of micro-constituents in HAZ. Therefore, this alloy's HAZ degradation is much more severe than that of non-heat-treatable alloys.

The severity of HAZ is generally expressed in terms of a softening factor, k_z. This factor represents the strength ratio in HAZ to the parent metal. In common practice, hardness mapping for identifying different zones resulting from the welding process can be implemented to evaluate HAZ. The hardness representation can clearly show the localisation of the softening zone and somehow allows the successful determination of yield stress and bulk modulus of specimens [4]. In accordance with Eurocode 9, the design value for the material in the HAZ can be defined as follows:

$$f_k z, d = k_z \frac{f_a}{Y_M} \quad (1)$$

Where f_a refers to the characteristic ultimate strength and γ_{M2}=1.25, which is the partial safety factor in tension or compression. However, this approximation is merely for conventional welding, such as MIG and TIG. Meanwhile, according to BS 8118 [5], HAZ's severity is generally determined by using the softening factor, which only depends on the alloy and tempered condition. In this case, the softening factor for welded EN AW 6082-T6 was taken to be 0.5 regardless of product form and welding method.

Meanwhile, the extent of the HAZ is significantly dependent on the welding heat input and material properties. A well-known method for estimating the extent of the HAZ is the "one-inch rule" [6], which is a sensible strategy for preliminary calculation before switching to a more scientific method for accuracy. For thinner material (thickness < 6mm), the extension of the HAZ could be considered radially from the centre of the weld root. It is estimated to be proportional to $\sqrt{A_w/n}$ and inversely proportional to the average thickness of the heat flow paths.

Early findings to explain the softening behaviour of aluminium alloys through numerical and experimental studies were made by Dumolt et al. [7] and Toshio [8]. They associated the softening behaviour of alloy with increasing ageing time and temperature. Since then, numerous studies have been done experimentally and numerically to investigate the mechanical behaviour and softening effects of weld joints in TIG [9-16] and laser welding [17-20]. Despite this, relatively few studies have focused specifically on the effects of the HAZ in welded joints

during TIG and laser beam welding of aluminium alloys like EN AW 6082-T6.

This study emphasises the effects of welding parameters on the occurrence of the heat-affected zone (HAZ) in the fusion welding process of TIG and laser beam on the aluminium alloy EN AW 6082-T6. Extensive experimental work, including the uniaxial tensile test, microhardness mapping, and metallographic investigations, was done to study the effect of mechanical properties and microstructural changes of the welded joint on the heat-affected zone of TIG and laser welding.

2.0 METHODOLOGY

The wrought base metals used in this study were commercial aluminium alloy EN AW 6082-T6 commonly used in structural applications such as structural components in cars, trusses system, and land-based structure. Plate thickness of the specimens was 4.75 mm. Consumable of ER 4043 was preferred in this current study, as it less sensitive to weld cracking and has a lower melting point. The consumable consists of 95% aluminium and 5% silicon, which become favourable for welding heat treatable alloys, specifically for 6000 series alloys. The chemical composition of the alloy and consumable was analyzed using energy-dispersive X-ray spectroscopy (EDX) and is given in Table 1.

Table 1: Chemical composition of base metal and consumable as measured by EDX analyzer.

Material	Chemical composition in wt %								
	Mn	**Fe**	**Mg**	**Si**	**Cu**	**Zn**	**Ti**	**Cr**	**Al**
EN AW 6082-T6	0.40	0.50	1.20	0.70	0.10	0.20	0.10	0.25	Balance
ER 4043	0.01	0.14	<0.01	5.00	0.02	0.01	0.01	<0.01	Balance

For the TIG welding experiment described here, the welding power source used was the Kemppi Master TIG MLS 2300 ACDC. The weld coupon was clamped in a fixture with a custom-made linear-moving table. Since the motion of welding torch and rod is not possible to directly automate, the use of movable linear-table can represent the

speed of welding by assuming that welding torch is in static state during welding process. The motion of linear-table was controlled using Arduino based program, and varied from 0.04 m/min to 0.23 m/min. The weld current was adjusted in several levels (120 A, 130 A, 132 A, 150 A) to allow a similar weld bead size. The input voltage was varied slightly in the range of 15.0 V to 19.0 V. Laser beam aluminium welding was conducted with a 6kW laser welding system. Consumable of ER 4043 was chosen for the filler material and the shielding gas is pure argon. The output laser power was varied in five (5) levels from 2.5kW to 4.5kW, and the welding speed was increased gradually from 0.9 m/min to 1.5 m/min.

Static tensile tests of the components were conducted in adherence to the ASTM E8/E8M-11. These tests were conducted at room temperature using a Shimadzu UTM testing machine. The tests conducted in two directions, 0◦ and 90◦, with reference to the extrusion direction. The displacement rate was maintained at a consistent 0.48 mm/min for all samples, ensuring the accuracy of our measurements. The elongation and displacement were recorded accordingly. The welded structure specimens were cut perpendicular to the weld line, with the weld centered in the section as seen in Figure 1, and the loading was normal to the welding direction. Specimens were extracted from the plate using wire electrical discharge machining (EDM). All samples were not polished to avoid any influence of surface roughness on plastic behaviour, further ensuring the reliability of our results.

Figure 1: Sub-size dogbone specimen (welded coupon) for tensile test

Micro-hardness testing was conducted to evaluate the material strength across the welding zones. The test was performed by impressing a precision diamond-shaped indenter with an angle of 136° onto the specimen's surface. Before the hardness testing, specimens were cut perpendicular to the weld bead for analysis. The flatness of the specimen's surface, a vital factor in the Vickers micro-hardness test,

was ensured through surface polishing before performing the indentations. A load of 200 g and a dwell time of 10 s were used for the micro-hardness testing. Indentations were made along the centre line of the chord member following a virtual mesh built with more than 200 nodes, according to the schematic representation shown in Figure 2. The distance between indentations varied depending on the welding region and methods. For TIG welded specimens, the indentation gap in HAZ was 0.5 mm, and the indentation gap was 1.0 mm in the base metal region. As the width of HAZ for the laser welded specimen is much less than that of the TIG specimen, the indentations were conducted at a 0.2 mm gap, considering only the 15 mm length of HAZ. The Vickers hardness *HV*, expressed in MPa, is calculated with respect to the true contact area:

$$H^V = 1.8544 \frac{P}{d^2} \tag{2}$$

where P is the applied load and d is the size of diagonal indentation.

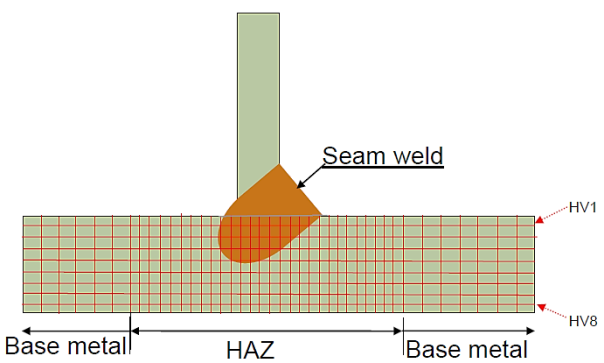

Figure 2: Schematic representation of virtual mesh for hardness mapping

To conduct micrographic analysis, specimens were prepared thoroughly per standard procedure. Specimens were subjected to mechanical grinding using silicon carbide (SiC) abrasive papers of 400, 600, 800, and 1200 grit. Six μm diamond paste was used for a rough polishing process, followed by final polishing on a woven pad using one μm of polycrystalline alumina (Al_2O_3). In order to reveal the grain boundary contrast in the welded specimens, the specimens were immersed in an etchant of Sodium Hydroxide NaOH solution and

heated to 60°C-70°C for about 15 minutes before being dipped in 65% nitric acid (HNO_3).

3.0 RESULTS AND DISCUSSION

3.1 Influence of Thermal Condition and Welding Speed on Mechanical Properties

The thermal condition of the TIG welding process was varied with the variation of heat input through a slight adjustment of input voltage and current. Meanwhile, thermal condition of laser welding was varied with the adjustment of nominal laser power. Figure 3(a) and (b) show the results of the influence of heat input on the ultimate strength and yield strength of TIG weldment coupons, respectively. A scatter was observed but the trend was clear. The least squares method was used to estimate the relation of heat input on ultimate tensile strength and yield strength. The fitted models (reported to two decimal places) were reported to be:

$$\text{ultimate tensile} = -8.56\ \text{heat input} + 176.10 \quad (3)$$

$$\text{yield strength} = -9.48\ \text{heat input} + 168.5 \quad (4)$$

with R^2 = 0.94 and R^2 = 0.98, respectively. The resulting equation's parameters indicate a linear correlation between heat input and output responses, suggesting that the ultimate strength and yield strength decrease as heat input increases.

The same tendency was observed in laser welding, as shown in Figure 4. However, there was no strong correlation between the responses and heat input parameters. Both cases show the reduction of mechanical strength with the increases in heat input. The reduction of mechanical responses was in accordance with the depletion of the strengthening mechanism. The mechanical strength of welded structures was primarily governed by their microstructural characteristics apart from the mechanical constraints. Thermal conditions influence the material's microstructure, which is heat input.

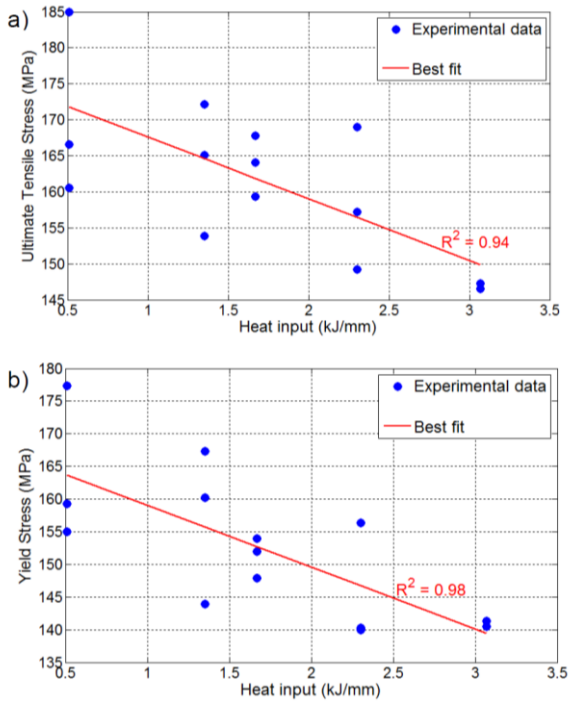

Figure 3: Influence of heat input on: (a) the ultimate strength; (b) yield stress of TIG weldment EN AW 6082-T6

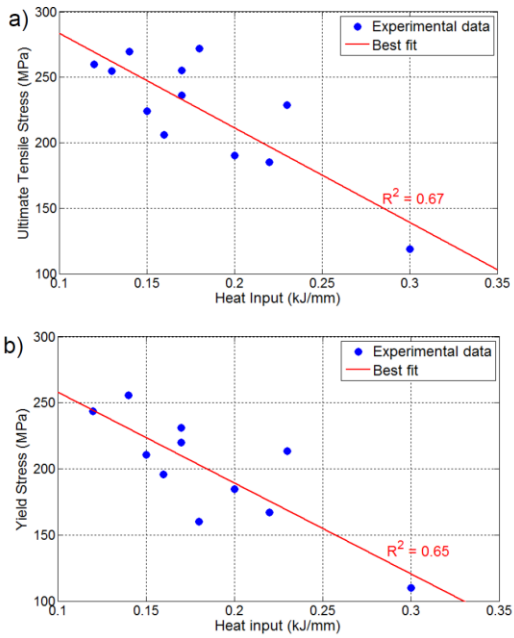

Figure 4: Influence of heat input on: (a) the ultimate strength; (b) yield stress of laser weldment EN AW 6082-T6

Comparing both cases of TIG and laser welding processes, the heat input amount differed. It is expected to be a higher amount of heat input in TIG welding than in laser welding due to the different power densities. Due to a larger consumable filler rod diameter, TIG poses a much lower power density than the laser welding process. Thus, with a bigger filler rod diameter, a bigger weld pool size was produced, and at the same time, the size of the HAZ became wider than necessary or not even fully fused. Meanwhile, for a fibre laser beam, the focal diameter is dependent on the fibre diameter and the optical system for collimating and focusing purposes.

The typical focal diameter in industrial laser welding ranges from 0.1 mm to 1.0 mm. Therefore, with a much higher power output (4.5 kW for the current study), a very high-power density (> 106 W/cm) was produced with even smaller HAZ, and substantial microstructural changes were not severe. Thus, higher mechanical strength can be attained. This is also the main reason that contributed to the good welding performance of laser-welded specimens. However, the reduction in mechanical strength for laser-

welded specimens was obviously inconsistent. It can be seen from Figure 4 that a significant drop was observed for 0.3 kJ/mm heat input. The strength reduction is almost 60% for both ultimate tensile stress and yield stress. In this case, the output power of the laser beam is the highest (4.5 kW) with the welding speed of 0.9 m/min (the lowest speed), which means the power density of this case was the highest among others. Penetration depth is inversely proportional to the speed for a constant power and focal diameter.

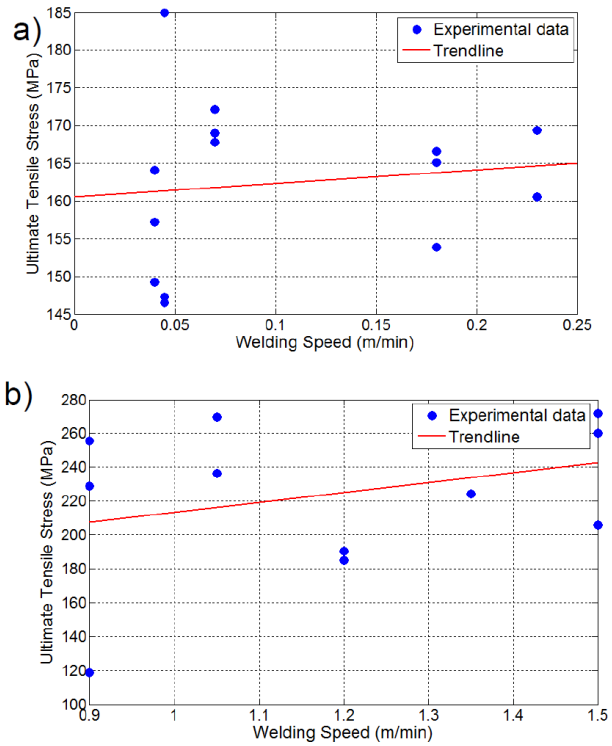

Figure 5: Effect of welding speed on ultimate tensile stress for (a) TIG welding cases; (b) laser welding cases of EN AW 6082-T6

Hence, a welding speed that is too low leads to excessive material melting, loss of material, and weld perforation and substantially causes a remarkable reduction in the tensile strength of joining components [21]. This phenomenon is in good agreement with the finding in the case of TIG welding, as illustrated in Figure 5(a). This finding was also observed in the case of laser welding (Figure 5(b)), in which a higher welding speed promotes a higher tensile stress.

Escalating the speed in welding provides a lower contact time of energy deposition, thus yielding a limited heat input to the weld zone. Consequently, less material was melted locally, inducing much narrower penetration, which is evident in Figure 6.

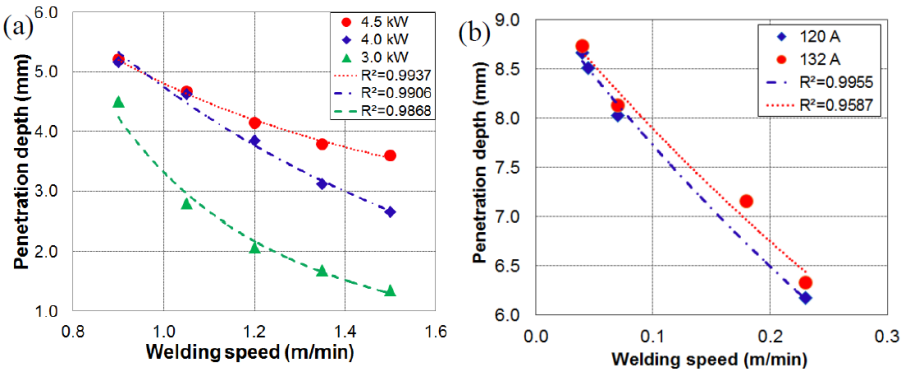

Figure 6: Effect of welding speed on penetration depth for: (a) laser welding cases; (b) TIG welding cases of EN AW 6082-T6

Compared to the base metal of EN AW 6082-T6, a remarkable reduction in tensile strength and yield stress was observed, as presented in Table 2 and Table 3. The presented data was the average mechanical strength values for each corresponding heat input and welding speed. The yield strength and tensile strength of the unwelded specimens were 256 MPa and 290.71 MPa, respectively, as obtained from the uniaxial tensile test. The ultimate strength of TIG welded components decreased by 40% - 50% [Table 2], whereas a broader range was obtained for laser welded specimens, accounting for an 11% to 60% reduction [Table 3]. The trend was also significant for the yield strength of the same components. The presence of alloying elements such as magnesium and silicon in ENAW 6082 contributes to the higher strength of the base metal. The primary strengthening mechanism is provided by the formation of precipitation of Mg_2Si, which significantly depends on temperature. However, since the precipitate is highly sensitive to the high-temperature environment (Temperature > 200°C), a significant drop in mechanical strength was observed in the welded specimens [22-25]. By introducing a filler metal (AA 4043), a large amount of silicon is available to form the precipitate. Conversely, the amount of

magnesium is lesser because magnesium is only present in the parent metal. Thus, fewer precipitates were found in the weld zone, resulting in a noticeable reduction of mechanical strength in the weld area compared to the base metal. The coarsening of the microstructure also contributes to the degradation of the mechanical properties at higher temperatures [26-28].

Table 2: Reduction in mechanical strength of TIG welded EN AW 6082-T6 (Calculated based on average value of each corresponding groups)

Condition	Ultimate strength, σ_T (MPa)	Reduction in σ_T (%)	Yield Strength, σ_Y (MPa)	Reduction in σ_Y (%)
Base metal	290.71	-	256.00	-
TIG-heat0.51*	170.71	41.28	163.85	36.00
TIG-heat1.35*	163.70	43.69	157.13	38.62
TIG-heat1.67*	163.76	43.67	151.27	40.91
TIG-heat2.30*	158.47	45.49	145.56	43.14
TIG-heat3.07*	146.88	49.48	140.91	44.96
TIG-speed0.04**	156.84	46.05	144.75	43.46
TIG-speed0.045**	159.58	45.11	153.04	40.22
TIG-speed0.07**	169.63	41.65	158.55	38.07
TIG-speed0.18**	161.86	44.32	154.47	39.66
TIG-speed0.23**	164.96	43.26	156.43	38.89

*heat input in kJ/mm **welding speed in m/min

Table 3**:** Reduction in mechanical strength of laser welded EN AW 6082-T6 (Calculated based on average value of each corresponding groups)

Condition	Ultimate strength, σ_T (MPa)	Reduction in σ_T (%)	Yield Strength, σ_Y (MPa)	Reduction in σ_Y (%)
Base metal	290.71	-	256.00	-
LB-heat0.12*	259.96	10.58	243.65	4.82
LB-heat0.15*	224.29	22.85	210.78	17.66
LB-heat0.17*	245.83	15.44	225.58	11.88
LB-heat0.22*	184.92	36.39	166.97	34.78
LB-heat0.30*	118.60	59.20	109.97	57.04
LB-speed0.90**	200.94	30.88	184.75	27.83
LB-speed1.05**	253.06	12.95	238.00	7.03
LB-speed1.20**	187.67	35.44	175.82	31.32
LB-speed1.35**	239.43	17.64	211.68	17.31
LB-speed1.50**	245.99	15.38	233.10	8.95

*heat input in kJ/mm **welding speed in m/min

3.2 Influence of Thermal Condition and Welding Speed on Microstructural Changes

The microstructure changes before and after the welding process are illustrated in Figure 7. From the SEM micrographs, the dimension of the grain size can be roughly estimated, and it was found that the grain size of unwelded EN AW 6082-T6 ranging between 20 μm to 70 μm. However, its dimension was significantly increased after the welding process, whereby the size ranged from 60 μm to 650 μm (TIG weldment) and 30 μm to 160 μm (laser weldment), depending on welding conditions. These measurements are based on manual grain size measurements [29], determined in the four sections of the weld area adjacent to FZ. The significant increase in the size of grains is closely related to the solidification behavior in the fusion zone.

Two factors that have a strong influence on the weld integrity were peak temperature and cooling rate. Based on Eq. 5, the cooling temperature rate is inversely proportional to the welding heat input:

$$\frac{dT}{dt} = -\left(\frac{2\pi kv}{\eta IV}\right)\left(T - T_0\right)^2 = C_1\frac{v}{Q} = \frac{C_1}{Q} \tag{5}$$

whereby k is thermal conductivity, v is velocity of heat source, η is arc efficiency, P is nominal power, T is temperature, T_0 is preheat temperature and Q is welding heat input ($Q = \eta P/v$). The peak temperature increases as the distance from the weld center decreases, thus allowing the microstructure to undergo significant changes. At higher exposure temperature (350-450°C), the precipitates are transformed into μm-size equilibrium β-Mg2Si particles [23]. The particle size is estimated from the following relationship;

$$\Delta D = be^{-Q/2RT_p}\left(t'\right)^n \tag{6}$$

The mathematical model in Eq. 6 describes grain growth during welding by knowing the activation energy, peak temperature, and time. The grain size will change according to peak temperature and time. Considering a higher peak temperature at the center of weld

region, this resulted in a slower cooling rate, which in turn coarsening the grain size in welded zone, as readily evident in Figure 7. The practical consequence of this coarsening is that a loss in mechanical strength in weld specimen. This effect was related to the Hall-Petch equation, where;

$$\sigma_T = \sigma_1 + k_y d^{-1/2} \tag{7}$$

From Eq. 7, the yield strength, σ_T of the weld specimen was reduced as the average diameter of grain, d increases, with the presence of constants, σ_1 and k_y. Although the strength loss due to grain growth in the aluminium alloy is merely a marginal effect, grain size does, however, have a significant effect on the risk of hot cracking.

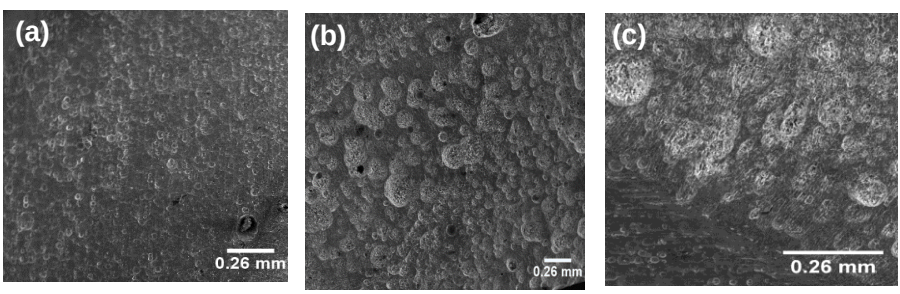

Figure 7: SEM micrographs showing the grain structure of: (a) unwelded specimen; (b) TIG welded specimen (heat input = 1.35 kJ/mm); (c) laser welded specimen of EN AW 6082-T6 (heat input = 0.3 kJ/mm)

Figure 8 shows the SEM results of the microstructural characteristic along the fusion line of the TIG welded specimen. Based on the result, it can be seen that the microstructure experienced transformation because the grains were coarse and equiaxed with non-epitaxial growth. Since the size, orientation, and distribution of the microstructure in the fusion zone are affected by the solidification behaviour of the molten pool, both FZ and PMZ exhibit different morphological structures. In the HAZ region, no apparent coarsening occurred. Instead, the equiaxed grains were forming into heterogeneous nucleation due to the rapid solidification process.

However, in the PMZ, the cellular grain growth appears to dominate the transformation. The cellular grains formed upwards and towards the fusion line, consistent with the high-temperature gradient towards the weld pool. Meanwhile, coarser grain was found in the FZ due to the higher peak temperature and slower cooling rate. Notice that the morphology of the structure was varies noticeably from the edge of the fusion line to the center of the weld region. A low growth rate along the fusion line is apparent as compared to the center of the weld, owing to the fact that the grain growth rate (G_R) is dependent on the temperature gradient (∇T). Since the ratio of $G_R/\nabla T$ decreases from the fusion line towards the center line of the weld, the solidification mode changes significantly from cellular to equiaxed grains across the PMZ and FZ [3,30].

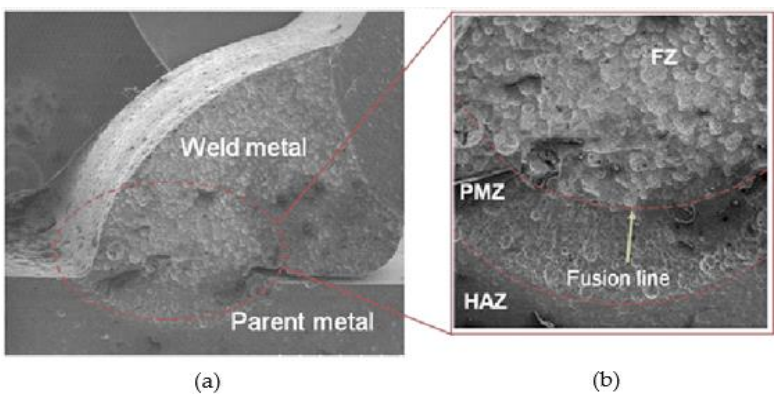

Figure 8: SEM micrograph of TIG-welded EN AW 6082-T6 (heat input = 1.35 kJ/mm) at: (a) 5X magnification; (b) 25X magnification

The morphological microstructure orientation of laser-welded EN AW 6082-T6 was further illustrated in Figure 9. As a fusion welding, three different zones were also formed during the laser welding process. From the figure, the clear fusion line between the fusion zone and HAZ can be seen. The fusion zone (FZ) was characterized by fine-grained microstructure. Contrary to the TIG welded specimen, the grain structure in the laser-welded specimen primarily consists of fine columnar dendrites originating from the fusion line with non-equiaxed grain growth in the weld centre. The partially-melted zone (PMZ) is typically very narrow. Thus, it cannot be distinguished in this specimen.

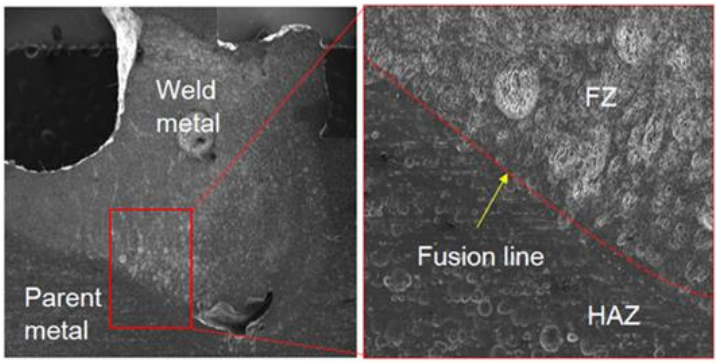

Figure 9: SEM micrograph of laser-welded EN AW 6082-T6 (heat input = 0.3 kJ/mm) at: (a) 5X magnification; (b) 25X magnification

3.3 Influence of Thermal Condition and Welding Speed on HAZ size

The results were represented as microhardness vs. distance measured from the weld root. Figure 10 illustrates the hardness mapping of both TIG and laser-welded specimens by the virtual mesh. From the figure, a clear trend can be observed, in which the hardness values were significantly reduced in HAZ, regardless of the distance across the thickness direction. Thus, it can provide strong evidence for the assumption of uniformity in temperature distribution through the plate thickness. In addition, an almost symmetric distribution of microhardness values can be seen on both sides of the weld region. Therefore, the hardness mapping for all specimens in this study was conducted only from the centre of the weld root in a single line across the mid-section of the thickness direction, considering the assumption above.

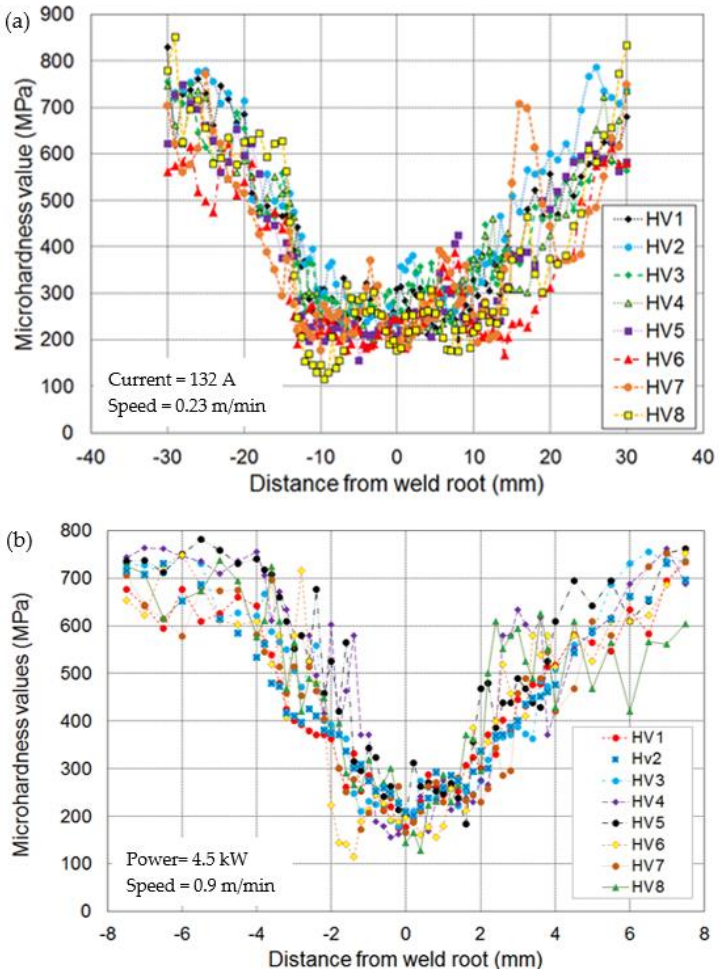

Figure 10: Hardness mapping in accordance to the virtual mesh of a (a) TIG welded specimen (b) laser welded specimen

In brief, the joint configuration, material thickness, peak temperature, preheat conditions and net energy input may influence the size of HAZ. For a thin plate with single-pass welding, the estimation width of HAZ is based on modified Rosenthal's equation of the simplified 3D heat flow equation. The cross-sectional geometry of weld bead and welding process parameters are related considering the following equations:

$$n_{ch} = \frac{Q_{rate} v}{4\pi\kappa^2 \rho C_p \left(T_m - T_o \right)} \tag{8}$$

$$D_{ch} = \frac{Y_{HAZ}{}^{V}}{4\kappa} \quad (9)$$

These parameters are essential for understanding how the rate of heat input and welding speed influence the temperature distribution during welding and heat-affected zone (HAZ) where the relationship of D_{ch} and n_{ch} can be found in literature [31]. Based on the equations, it is clear that heat input rate has a positive correlation with the size of HAZ. Hence, a heat input in laser welding will eventually promote lesser dissolved precipitates and thereby providing narrowed softened regions (HAZ).

To estimate the size of HAZ, T_m can be substituted by the critical temperature, in which the temperature of some relevant phase transformation that could take place. In this study, EN AW 6082-T6 is subjected to the metallurgical transformation above 220◦C, i.e. the lower critical temperature [32]. In the case of 0.3 kJ/mm heat input in laser welding, the estimated value of HAZ (based on Eq. 8 and Eq. 9) was 6.13 mm (full width). This estimation was underestimated at almost 14.8% for this case, in which the mapped hardness profile was found to be 3.6 mm for the one-sided welded region (full HAZ width = 7.2 mm), as depicted in Figure 11. The calculated value was slightly lower from the experimental value because the material properties were assumed to be constant with varying temperature, i.e. thermal properties do not change during the welding process.

To quantitatively evaluate the effect of the heat input on the size of HAZ, a careful mapping of the hardness profile on laser-welded specimens of different heat input levels was performed. The results are presented in Table 4, which indicates that the width of HAZ was affected slightly with the increase of the heat input.

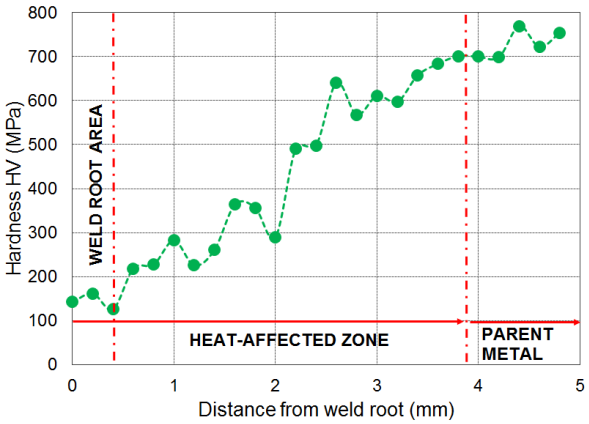

Figure 11: The hardness mapping of a laser welded specimen for the case of heat input = 0.3 kJ/mm

Table 4: The width of HAZ for varying heat input in the case of laser welded EN AW 6082-T6

Heat input / $kJmm^{-1}$	*App. width of HAZ (full width) / mm	**Est. width of HAZ (full width) / mm	% of difference	Lowest microhardness value in HAZ / MPa
0.12	5.60	5.44	2.86	196.51
0.14	6.00	5.60	6.67	190.85
0.20	6.40	5.57	12.91	192.24
0.23	6.80	5.76	15.34	161.54
0.30	7.20	6.13	14.80	141.95

* Obtained from experimental analysis.
** Calculated based on Eq. 7 and Eq. 8.

To relate the hardness with the volume of a fraction of precipitates, a relation has been quantitatively proposed in [32], as follows:

$$1 - X = \frac{f}{f_0} = \frac{HV - HV_{min}}{HV_{max} - HV_{min}} \quad (10)$$

where X is the fraction of dissolved precipitates in matrix, f is volume fraction of strengthening β'' precipitates, f_0 is initial volume fraction of strengthening β'' precipitates, HV is the Vickers hardness, HV_{max} is the base metal hardness in T6 condition and HV_{min} is the minimum hardness in the absence of hardening precipitates. HV_{max} and HV_{min}

were obtained from experimental data and the values are 756.82 MPa and 141.97 MPa, respectively. By using Eq. 10 the hardness distributions in the HAZ in terms of f/f_0 can be obtained, as shown in Figure 12.

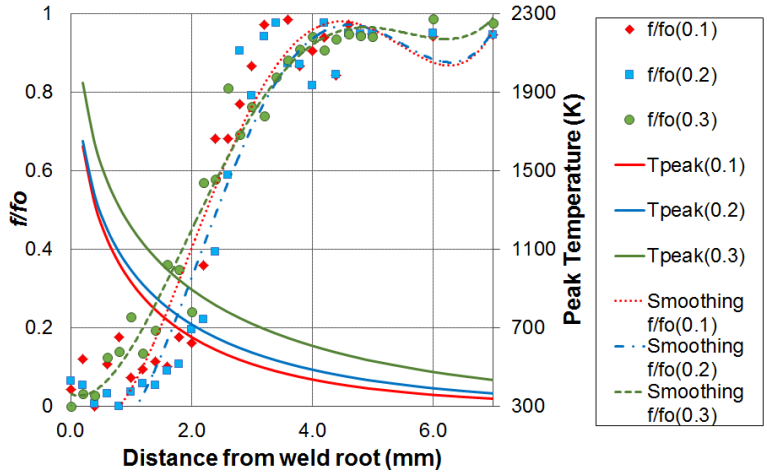

Figure 12: Distribution of f/f_0 and peak temperatures in HAZ for laser welded specimens of EN AW 6082-T6

The peak temperature distribution in HAZ as shown in the Figure 12 was calculated from the modified Rosenthal's equation [33];

$$T - T_o = \frac{q_o / h}{2\pi\lambda} \exp\left(-\frac{vx}{2\kappa}\right) K_o\left(\frac{vr}{2\kappa}\right) \tag{11}$$

The equation provides an understanding of how the heat from the laser source affects the temperature distribution, including HAZ, at various locations in the material. The equation calculated temperature distribution in a plate during laser welding, considering the material properties such as conductivity and diffusivity, incident power of laser beam, and welding speed. For actual prediction, the absorptivity of the incident power was determined by comparing the measured thermal cycle with the calculated thermal cycle with the varied q_o. The absorptivity of the laser beam in this study was 0.5. From the figure, the softened regions were defined as the regions where hardness values fall below 90% of the base metal hardness [34,35], which is, in

this case, within 4.0 mm from the weld root. This result is quite similar with the findings in [34,35], where the widths of softened regions in the HAZs of the laser beam welds were 1/7 to 1/4 that of the TIG welds. The hardness mapping was also implemented on all other specimens of TIG welded coupons. Experimental evidence for the curvature in terms of hardness impressions concerning the distance measured from the weld root for various heat inputs was given in Figure 13 for TIG welded specimens.

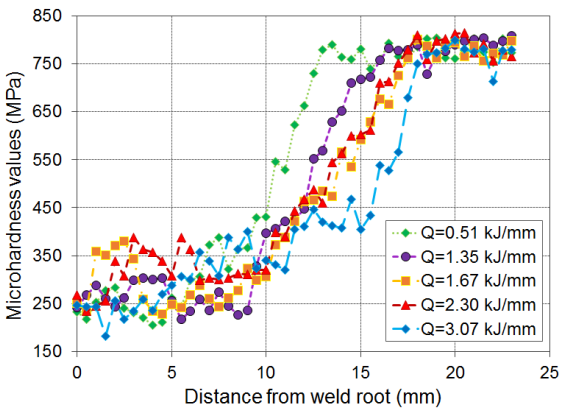

Figure 13: The effect of heat input on the width of HAZ for TIG welded specimens of EN AW 6082-T6

A clear trend of a significant drop in hardness values toward the weld root can be seen in Figure 13. In the case of TIG welded specimens, the width of HAZ ranged from 25 mm to 35 mm (measured in full width), depending on the heat input. A series of hardness mapping plots in terms of f/fo for TIG welded specimens were illustrated in Figure 14. From the figures, the softened region can readily be determined by a significant drop of 90% from maximum hardness, which is within 17 mm from the weld root. The distribution of the peak temperature was calculated based on Eq. 11 with $q_o = \eta P_L$ (η is the thermal efficiency). To facilitate the actual prediction, η was taken to be 0.6 (TIG specimens). Note that the lower critical temperature for metallurgical transformation of this alloy was determined previously [36] and taken to be at 220℃ (≈493K). Therefore, the lower critical temperature should be within the range of the softened region. In Figure 14, the lower critical temperature was found within the desired range (in the range of 12 mm - 17 mm from the weld root), which is in a good

agreement with the finding. Thus, this argument facilitated the clear evident that the size of HAZ was slightly affected by the heat input.

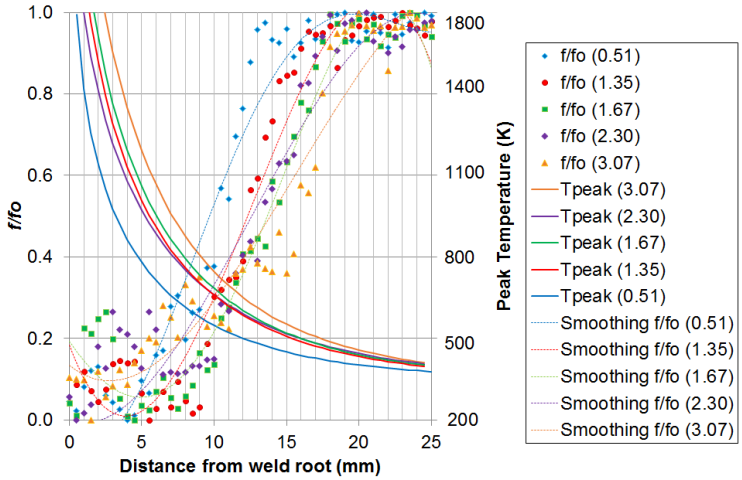

Figure 14: Distribution of f/f_0 and peak temperatures in HAZ for TIG welded specimens of EN AW 6082-T6

To demonstrate the effect of welding speed on the size of HAZ, a series of HAZ sizes were plotted against the speed in all welding cases, as depicted in Figure 15. A clear trend can be observed from all cases in which the size of HAZ decreases as the welding speed increases. Based on the results, increasing the welding speed leads to a lower contact time of energy deposition, causing low heat input to the weld zone. This, in turn, affects the peak temperature and thus influences the isotherm contour during welding. This argument was also supported by Eq. 11, whereby the welding speed was written in the form of exponential decay and Bessel function (modified second order). Therefore, the welding speed and heat input have a contrary effect on the size of HAZ.

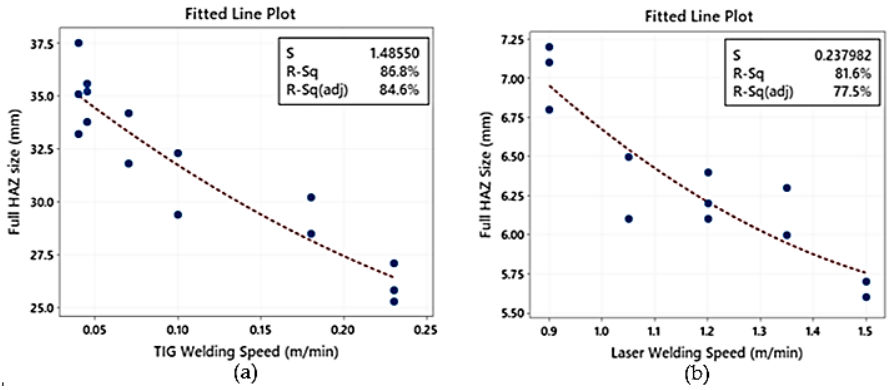

Figure 15: The effect of welding speed on the size of HAZ for (a) TIG and MIG and (b) laser welding of EN AW 6082-T6

4.0 CONCLUSION

This study focuses on the experimental and numerical analysis of welded aluminium structures, particularly the HAZ. The softening phenomenon due to the welding process was well understood by comparing the mechanical performance and microstructural morphology of fusion welding methods, particularly TIG and laser beam welding. From the results, it was concluded that:

- The ultimate tensile stress and yield stress of welded components decrease with the increases in heat input, while the mechanical strengths of welded components increase with the increase of welding speed, regardless of welding method. An inconsistent trend was observed in the mechanical responses of laser-welded joints, with the values of strength reduction ranging from 11% - 60%. However, in contrast, the reduction in mechanical strength of TIG welded components was more consistent with the values ranging from 40% - 50%.
- The study revealed significant changes in the grain size and orientation after the welding process. Depending on the welding method, the grain size after welding ranged from 60 μm to 650 μm (TIG weldment) and 30 μm to 160 μm (laser weldment). The orientation of the grain was found to be different for each welding method and was greatly influenced by the welding speed and temperature gradient of the weld pool. These changes in the

microstructure may contribute to a reduction in the mechanical strength of the welded joint, as the strength loss is dependent on the average grain diameter.

- The size of HAZ increases with the increase of heat input regardless of the welding method. In the case of TIG welded specimens, the width of HAZ ranged from 25 mm to 35 mm (measured in full width), depending on the heat input. Much narrower HAZ size was reported in the case of laser welded components, in which the full width of HAZ ranged from 5.6 mm to 7.2 mm.

This work compares mechanical properties and microstructural changes in TIG and laser-welded components, which can provide a basis for further improving the current design and welding joining standards, particularly the softening factor of welded joining. The results of this study will significantly contribute to the enhancement of welding quality in industrial joining practice.

ACKNOWLEDGMENTS

Special acknowledgement to Universiti Teknikal Malaysia Melaka (UTeM) and Universiti Sains Malaysia (USM) for the financial support. The authors acknowledge the support from the Malaysian Ministry of Education (MoE). This research was funded through a research grant of PJP/2022/FKP/S01870 (UTeM) and 1001/PMEKANIK/814235 (USM). Special Thanks to SIMTech Singapore for the technical support and sample preparation.

AUTHOR CONTRIBUTIONS

Material preparation and data collection were performed by Imam Fauzi E.R. Data Analysis and interpretation were performed by Elfi ER and Najib A.M. The first draft of manuscript was written by Imam Fauzi ER and improved by Najib A.M. All authors commented on previous versions of the manuscript. All authors read and approved the final version of the manuscript. B. Umroh and M.S. Rusdi read, writing-reviewing and approved the final version of the manuscript.

CONFLICTS OF INTEREST

The manuscript has not been published elsewhere in any journal publisher and is not under consideration by other journals. All authors have approved the review, agree with its submission and declare no conflict of interest on the manuscript.

REFERENCES

[1] T. Sun, P. Franciosa, M. Sokolov and D. Ceglarek, "Challenges and opportunities in laser welding of 6xxx high strength aluminium extrusions in automotive battery tray construction", *Procedia CIRP*, vol. 94, pp. 565-570, 2020.

[2] B. Ivan, OM. Akselsen, X. Ren, B. Nyhus, M. Eriksson and S. Gulbrandsen-Dahl. "A Review on Laser-Assisted Joining of Aluminium Alloys to Other Metals" *Metals*, 11, no. 11, pp.1680, 2021.

[3] E. R. Imam Fauzi, M. S. C. Jamil, Z. Samad and P. Muangjunburee, "Microstructure analysis and mechanical characteristics of tungsten inert gas and metal inert gas welded AA6082-T6 tubular joint: A comparative study", *Transactions of Nonferrous Metals Society of China*, vol. 27, no. 1, pp. 17-24, 2017.

[4] R. R. Ambriz, D. Chicot, N. Benseddiq, G. Mesmacque and S. D. de la Torre, "Local mechanical properties of the 6061-T6 aluminium weld using micro-traction and instrumented indentation", *European Journal of Mechanics - A/Solids*, vol. 30, no. 3, pp. 307-315, 2011.

[5] British Standard Institution, British Standard BS 8118: Part 1: 1991. London, 1991.

[6] G. Mathers, *The welding of aluminium and its alloys*. CRC Press, London: Woodhead Publishing Limited, 2002.

[7] S. D. Dumolt, D. E. Laughlin and J. C. Williams, "Formation of a modified β′ phase in aluminum alloy 6061", *Scripta Metallurgica*, vol. 18, no. 12, pp. 1347-1350, 1984.

[8] E. Toshio and K. Toshio, "Microstructure in weld heat affected zone of Al-Mg-Si alloy", *Transactions of JWRI (Japanese Welding Research Institute)*, vol. 11, no. 61, pp. 61–66, 1982.

[9] M. Matusiak and P. K. Larsen, "*Strength and ductility of welded connections in aluminium alloys joints"*, in Aluminium-INALCO, 1999, pp.99-309.

[10] W. Feng, Y. Li, X. Chen, H. Zhao, K. Yaqoob, Y. Du, Z. Wang, and M. Song, "Superior Strength–Ductility Combination in Al Alloys via Dislocation Gradient Structure", *Materials Research Letters*, vol. 11, no. 5, pp. 347–53, 2022.

[11] T. K. Chan and R. F. D. Porter Goff, "Welded aluminium alloy connections: test results and BS8118", *Thin-Walled Structures*, vol. 36, no. 4, pp. 265-287, 2000.

[12] Z. L. Zhang, J. Ødegård, O. R. Myhr and H. Fjær, "From microstructure to deformation and fracture behaviour of aluminium welded joints – a holistic modelling approach", *Computational Materials Science*, vol. 21, no. 3, pp. 429-435, 2001.

[13] O. R. Myhr, Ø. Grong, H. G. Fjær and C. D. Marioara, "Modelling of the microstructure and strength evolution in Al–Mg–Si alloys during multistage thermal processing", *Acta Materialia*, vol. 52, no. 17, pp. 4997-5008, 2004.

[14] O. R. Myhr, O. S. Hopperstad and T. Børvik, "A Combined Precipitation, Yield Stress, and Work Hardening Model for Al-Mg-Si Alloys Incorporating the Effects of Strain Rate and Temperature", *Metallurgical and Materials Transactions A*, vol. 49, no. 8, pp. 3592 – 3609, 2018.

[15] M. Touboul, J. Crepin, G. Rousselier, F. Latourte and S. Leclercq, "Identification of Local Viscoplastic Properties in P91 Welds from Full Field Measurements at Room Temperature and 625 °C", Experimental Mechanics, vol. 53, no. 3, pp. 455- 468, 2013.

[16] A. Bansal, M. Senthil Kumar, I. Shekhar, S. Chauhan and S. Bhardwaj, "Effect of welding parameter on mechanical properties of TIG welded AA6061", *Materials Today: Proceedings*, vol. 37, no. 2, pp. 2126-2131, 2021.

[17] A. C. Oliveira, R. H. M. Siqueira, R. Riva and M. S. F. Lima, "One-sided laser beam welding of autogenous T-joints for 6013-T4 aluminium alloy", *Materials & Design*, vol. 65, pp. 726-736, 2015.

[18] C. Zhang, M. Gao and X. Zeng, "Effect of microstructural characteristics on high cycle fatigue properties of laser-arc hybrid

welded AA6082 aluminum alloy", *Journal of Materials Processing Technology*, vol. 231, pp. 479-487, 2016.

[19] P. K. Arya, V. Kumar, D. Sathiaraj, I. A. Palani, N. K. Jain, "Microstructural and Mechanical Properties Analysis of Fibre Laser Welding of Dissimilar AA6061 and AA2024 Aluminium Alloy", Recent Advances in Manufacturing Processes and Systems, *Lecture Notes in Mechanical Engineering*, pp.681-688, 2022.

[20] A. Faye, Y. Balcaen, L. Lacroix and J. Alexis, "Effects of welding parameters on the microstructure and mechanical properties of the AA6061 aluminium alloy joined by a Yb: YAG laser beam ", *Journal of Advanced Joining Processes*, vol. 3, no. 100047, 2021.

[21] S. Miroslav, P. Marián, S. Martin, K. Pavel and M. Maroš, "Effect of Travel Speed on the Properties of 5087 Aluminum Alloy Walls Produced by Wire and Arc Additive Manufacturing", *Journal of Materials Engineering and Performance*, vol. 33, no. 16, pp. 8582 - 8600, 2024.

[22] C. Sigli, F. D. Geuser, A. Deschamps, J. Lépinoux and M. Perez, "Recent advances in the metallurgy of aluminum alloys. Part II: Age hardening", *Comptes Rendus Physique*, vol. 19, no. 8, pp. 688-709. 2018.

[23] A. K. Gupta, D. J. Lloyd, S. A. Court, "Precipitation hardening in Al–Mg–Si alloys with and without excess Si", *Materials Science and Engineering: A*, vol. 316, no. 1–2, pp. 11-17, 2001.

[24] X. Fang, M. Song, K. Li and Y. Du, "Precipitation sequence of an aged Al-Mg-Si Alloy", *Journal of Mining and Metallurgy B: Metallurgy*, vol. 46, no. 2, pp. 171–180, 2010.

[25] R. Jovid, K. Liu, P. Rometsch, N. Parson, and X.-Grant Chen, "Improving the Mechanical Response of Al–Mg–Si 6082 Structural Alloys during High-Temperature Exposure through Dispersoid Strengthening" *Materials*, vol. 13, no. 22, pp. 5295, 2020.

[26] P. T. Summers, Y. Chen, C. M. Rippe, B. Allen, A. P. Mouritz, S. W. Case, and B. Y. Lattimer, "Overview of aluminum alloy mechanical properties during and after fires", *Fire Science Reviews*, vol. 4, no. 3, 2015.

[27] J. Maljaars, F. Soetens and L. Katgerman, "Constitutive Model for Aluminum Alloys Exposed to Fire Conditions", *Metallurgical and Materials Transactions A*, vol. 39, no. 4, pp. 778 - 789, 2008.

[28] C. T. Gross, D. Isheim, S. Vaynman, M. E. Fine, and Y. W. Chung,

"Design and Development of Lightly Alloyed Ferritic Fire-Resistant Structural Steels", *Metallurgical and Materials Transactions A*, vol. 50, no. 1, pp. 209 - 219, 2019.

[29] ASTM International, E112-12: Standard test methods for determining average grain size, ASTM International, West Conshohocken: US, 2012.

[30] Q. Wu, J. Li, L. Long, and L. Liu "Simulating the Effect of Temperature Gradient on Grain Growth of 6061-T6 Aluminum Alloy via Monte Carlo Potts Algorithm," *Computer Modeling in Engineering & Sciences*, vol. 129, no. 1, pp. 99-116, 2021.

[31] N. Christensen, V. L. Davies and K. Gjermundsen, "Distribution of temperatures in arc welding", *British Welding Journal*, vol. 12, no. 12, pp. 54-75, 1965.

[32] O. R. Myhr and Ø. Grong, "Process modelling applied to 6082-T6 aluminium weldments—I. Reaction kinetics", *Acta Metallurgica et Materialia*, vol. 39, no. 11, pp. 2693-2702, 1991.

[33] A. Hirose, K. F. Kobayashi, and H. Todaka, "CO2 laser beam welding of 6061-T6 aluminum alloy thin plate", *Metallurgical and Materials Transactions A*, vol. 28, no. 12, pp. 2657 - 2662, 1997.

[34] A. Hirose, K. F. Kobayashi, H. Yamaoka H. and N. Kurosawa, "Evaluation of properties in laser welds of A6061-T6 aluminum alloy", *Welding International*, vol. 14, no. 6, pp. 431- 438, 2000.

[35] A. Hirose, N. Kurosawa, K. F. Kobayashi, H. Todaka and H. Yamaoka, "Quantitative evaluation of softened regions in weld heat-affected zones of 6061-T6 aluminum alloy—Characterizing of the laser beam welding process", *Metallurgical and Materials Transactions A*, vol. 30, no. 8, pp. 2115- 2120, 1999.

[36] B. I. Bjørneklett, Ø. Grong, O. R. Myhr and A. O. Kluken, "A process model for the heat-affected zone microstructure evolution in Al-Zn-Mg weldments", *Metallurgical and Materials Transactions A*, vol. 30, no. 10, pp. 2667 - 2677, 1999.